Report

Cell Reports

# Transcription Factor Binding to Replicated DNA

## Graphical Abstract

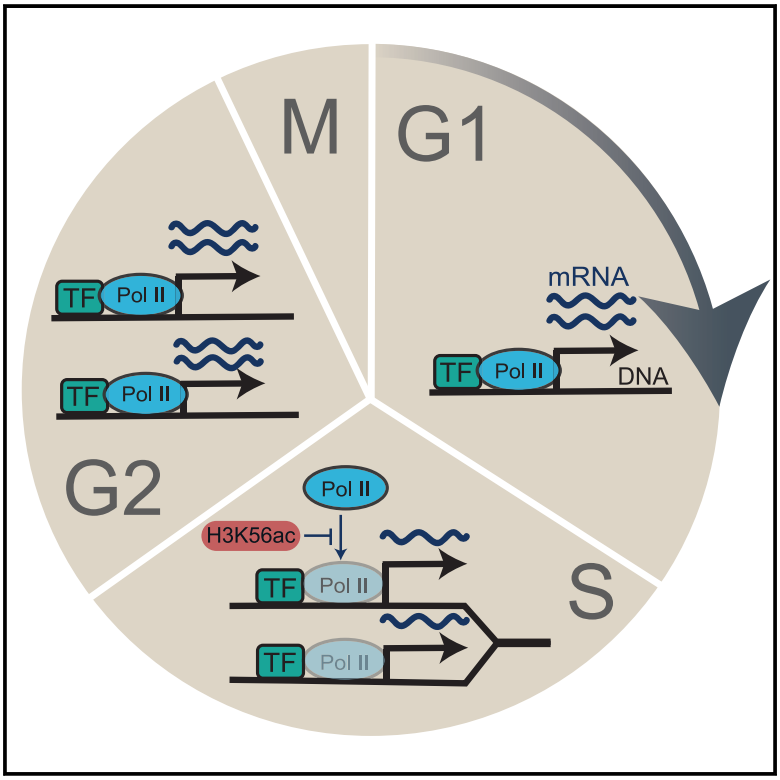


## Authors

Raz Bar-Ziv, Sagie Brodsky, Michal Chapal, Naama Barkai

## Correspondence

naama.barkai@weizmann.ac.il

## In Brief

During genome replication, mRNA synthesis from replicated genes is inhibited. Bar-Ziv et al. find that transcription factors (TFs) are recruited to replicated promoters but RNA polymerase II (Pol II) binding is buffered. Their work suggests that the unique chromatin environment during DNA replication limits the ability of TFs to recruit Pol II.

## Highlights

- The binding of Pol II and TFs to DNA was measured during S phase in budding yeast
- TFs are temporally evicted from replicated promoters but regain binding rapidly
- TF binding to replicated DNA is proportional to the increase in DNA content
- The ability of TFs to recruit Pol II is limited by the chromatin environment

Bar-Ziv et al., 2020, Cell Reports *30*, 3989–3995
March 24, 2020 
https://doi.org/10.1016/j.celrep.2020.02.114

CellPress

Cell Reports
Report



# Transcription Factor Binding to Replicated DNA

Raz Bar-Ziv,[1,2,3] Sagie Brodsky,[1,3] Michal Chapal,[1] and Naama Barkai[1,4,*]
[1]Department of Molecular Genetics, Weizmann Institute of Science, Rehovot 76100, Israel
[2]The Howard Hughes Medical Institute, University of California Berkeley, Berkeley, CA 94720, USA
[3]These authors contributed equally
[4]Lead Contact
*Correspondence: naama.barkai@weizmann.ac.il
https://doi.org/10.1016/j.celrep.2020.02.114

## SUMMARY

**Genome replication perturbs the DNA regulatory environment by displacing DNA-bound proteins, replacing nucleosomes, and introducing dosage imbalance between regions replicating at different S-phase stages. Recently, we showed that these effects are integrated to maintain transcription homeostasis: replicated genes increase in dosage, but their expression remains stable due to replication-dependent epigenetic changes that suppress transcription. Here, we examine whether reduced transcription from replicated DNA results from limited accessibility to regulatory factors by measuring the time-resolved binding of RNA polymerase II (Pol II) and specific transcription factors (TFs) to DNA during S phase in budding yeast. We show that the Pol II binding pattern is largely insensitive to DNA dosage, indicating limited binding to replicated DNA. In contrast, binding of three TFs (Reb1, Abf1, and Rap1) to DNA increases with the increasing DNA dosage. We conclude that the replication-specific chromatin environment remains accessible to regulatory factors but suppresses RNA polymerase recruitment.**

## INTRODUCTION

DNA serves as a common template connecting gene transcription and genome replication, two fundamental cellular processes. Transcription and replication both depend on the ability of regulatory factors to access DNA and progress smoothly along the genome. The accessibility of DNA to regulatory factors is limited by its wrapping around histone octamers, which form nucleosomes, the basic building blocks of chromatin. DNA accessibility is not uniform across the genome but depends on multiple elements, including the DNA sequence, regulatory factors present at adjacent regions, and modifications added to histone tails, all of which could affect the affinity of DNA to histones. Inevitably, this makes the chromatin environment a major effector of transcription and replication, explaining the extensive regulation of this environment during both processes (Bannister and Kouzarides, 2011; MacAlpine and Almouzni, 2013).

DNA replication challenges the stability of gene expression at several levels. First, replication introduces gene dosage imbalance, simply because replicated genes have double DNA dosage relative to those yet to replicate. Second, encounters between the progressing replication fork and DNA-bound transcription factors (TFs), or transcribing RNA polymerases, may impinge on both processes. Furthermore, replication perturbs the epigenetic landscape by directly modifying histones and by introducing new histones that carry a unique, position-independent set of marks (Ramachandran et al., 2017). Some marks recover their pre-replication pattern rapidly, but others recover slowly, over a period that can extend beyond S phase (Alabert et al., 2015; Bar-Ziv et al., 2016a). Finally, nucleosome positions are altered as histones are evicted by the replication fork and regain their pre-replication distribution with some delay (Fennessy and Owen-Hughes, 2016; Ramachandran and Henikoff, 2016; Vasseur et al., 2016). Therefore, during DNA replication, gene transcription proceeds in a unique DNA environment that is different from the environment it encounters outside of S phase.

In bacteria, the gene-dosage imbalance introduced during DNA replication results in increased transcription of replicated genes, an effect incorporated into bacterial gene-regulatory strategies (Slager and Veening, 2016). Eukaryotes, however, buffer this imbalance by suppressing transcription from replicated DNA (Yunger et al., 2010; Padovan-Merhar et al., 2015; Bar-Ziv et al., 2016b). We recently showed that, in budding yeast, buffering depends on acetylation of H3K56 by the acetyltransferase Rtt109 (Voichek et al., 2016) and on H3K4 methylation by the Paf1-recruited COMPASS complex (Voichek et al., 2018). H3K56ac is deposited in replicated regions (Driscoll et al., 2007; Han et al., 2007) and H3K4me3, which is associated with active transcription, decreases in replicated regions (Voichek et al., 2018). Notably, in the case of replication stress, this feedback is stabilized by the DNA replication checkpoint, underlining its functional relevance. Therefore, although the increased dosage of replicated genes can potentially lead to increased transcription, it is suppressed by the epigenetic landscape characterizing replicated DNA. The suppression of transcription from replicated DNA could result from the limited ability of regulatory factors to access the DNA at these regions. Alternatively, it could result from a more specific inhibition of the transcription machinery itself. Here, we set to distinguish between these possibilities by examining the unperturbed replication dynamics of the two intermediate layers connecting the chromatin environment to gene expression: binding of RNA polymerase II (Pol II) to replicated DNA and binding of TFs to their *cis*-regulatory elements in replicated gene promoters.

We followed budding yeast progressing through unperturbed S phase, profiling, at high temporal resolution, the genome-wide binding of Pol II and three TFs that have a large number of binding targets: Reb1, Abf1, and Rap1. We found little evidence

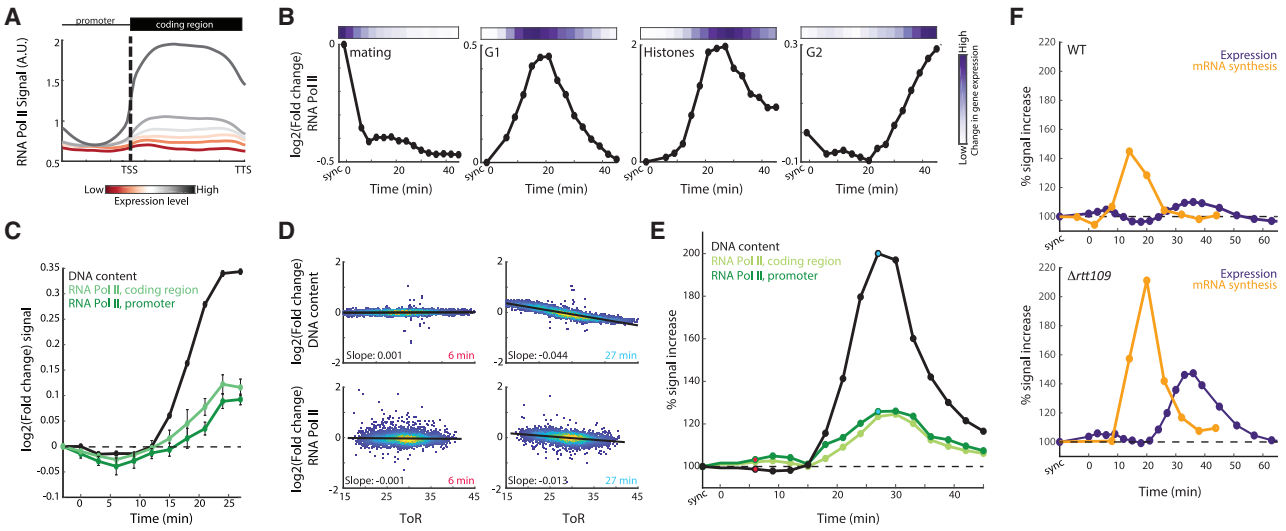


**Figure 1. Genomic Localization of Pol II during DNA Replication**

(A) Pol II binding correlates with gene expression. Genes were classified into 6 groups based on expression levels, aligned by their transcription start and termination sites (TSS and TTS, respectively; defined in David et al., 2006), and binned to control for gene length. Shown is the binding profile of Pol II, averaged over each group. See also Figures S1A and S1C–S1E.

(B) Temporal changes in Pol II correlate with changes in mRNA expression. The average fold change in binding of Pol II to open reading frames (ORFs) of the indicated gene groups is shown following the release from G1 arrest (bottom). The corresponding gene expression change, as quantified in Voichek et al. (2016), is shown as a color code (top). See also Figure S1B.

(C) Pol II binding to early replicating genes. Pol II binding intensities and DNA abundance were log-normalized by the G1-arrested time point and averaged over the 200 earliest replicating genes. Shown are the respective averages and the standard error (SE), following release from G1 arrest.

(D) Temporal progression of DNA replication. Individual panels depict the fold change in DNA content (top) or Pol II binding (bottom), normalized by the G1 arrest time point, as a function of the respective ToR. Each dot represents a gene. Note the uniform behavior at early times, before replication starts, compared to later times, when cells have replicated part of their genome. This dependency between the measured parameter (DNA content or Pol II binding) and ToR (as defined by Yabuki et al., 2002) is quantified by the respective slopes.

(E) Minor sensitivity of Pol II to gene dosage. Shown is the dependency of Pol II binding on ToR, calculated on all genes with an annotated TSS (David et al., 2006), quantified as in (D) and normalized by the corresponding dependency of DNA content in mid-S-phase (STAR Methods; Figure S1E). The red and blue dots correspond to the time points shown in (D).

(F) A complete loss of transcription buffering in RTT109-deleted cells. The change in mRNA expression and mRNA synthesis rate, calculated as described in (D) and (E), for wild-type (top) and *Δrtt109* (bottom). mRNA synthesis rate was calculated as previously described in Voichek et al. (2016).

for a replication-associated depletion of Pol II from DNA, suggesting that, if evicted by the progressing fork, it resumes binding rapidly. Furthermore, the increase in DNA content during replication had only a minor effect (~20%) on Pol II binding to replicated genes or promoters. In contrast, the transient depletion of the three TFs examined from replicating regions was more pronounced. These factors then regained binding, increasing in abundance with the increasing DNA content of replicated regions to an extent that was at least proportional to the increase in DNA dosage. Together, our data suggest that the unique chromatin environment introduced during replication does not prevent TF binding but does suppress the ability of these factors to recruit Pol II and initiate gene transcription.

## RESULTS

### The Pattern of Pol II Binding to DNA during S Phase

Replication can perturb the genomic distribution of Pol II binding in at least two ways. First, Pol II could be transiently evicted by the replication fork. Second, Pol II binding may increase in replicated regions, whose DNA dosage increases, at the expense of other regions yet to replicate.

To examine the extent to which DNA replication perturbs Pol II binding to DNA, we analyzed our previously published data of Pol II binding in cells progressing synchronously through S phase (Bar-Ziv et al., 2016a). In this experiment, we released budding yeast from α-factor-induced arrest at the end of G1 and sampled at 3-min intervals to profile DNA replication by DNA sequencing and Pol II binding by chromatin immunoprecipitation sequencing (ChIP-seq). We verified the synchronous progression of the cells through S phase by DNA staining and observed the expected correlation between Pol II occupancy and absolute expression levels, as well as the expected temporal changes in binding to the regulated cell-cycle gene groups (Figures 1A, 1B, and S1).

To examine whether the progressing replication fork coincides with eviction of Pol II from regions being replicated, we considered early-replicating regions, as defined by data quantifying the time at S phase at which each genomic region is replicated (time of replication [ToR]) (Yabuki et al., 2002). Quantifying DNA content in these regions, we observed the expected increase shortly after release from α-factor arrest (Figure 1C). In contrast, Pol II binding was largely stable, showing only a minor transient reduction in binding to these regions. Therefore, within our temporal resolution (~3 min), we could not detect a significant

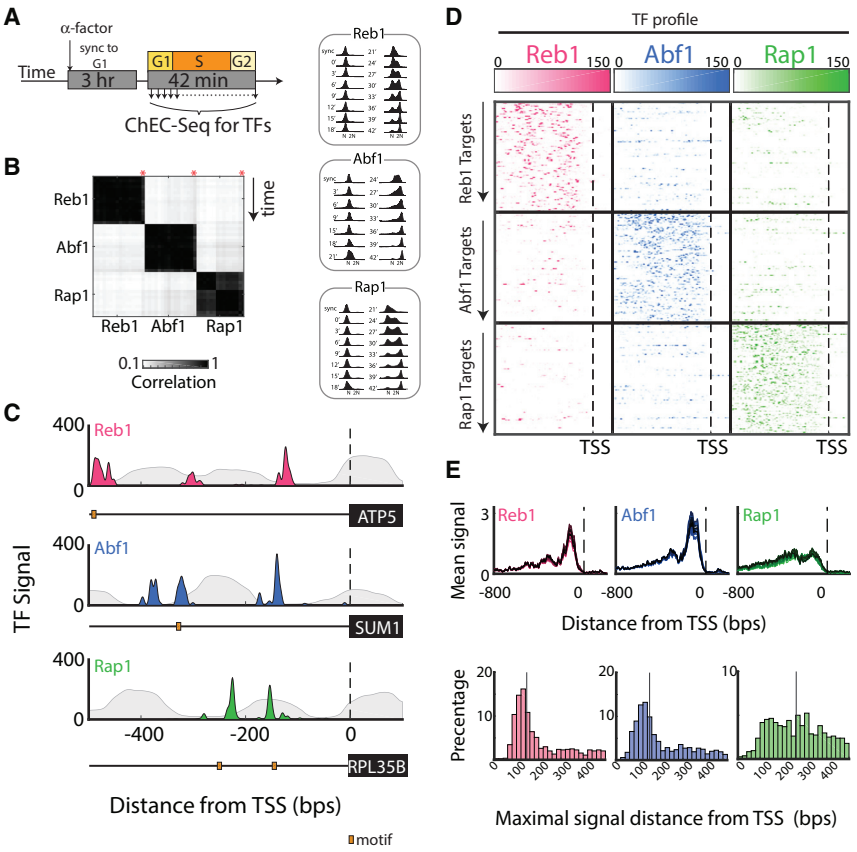


**Figure 2. Genomic Localization of the Transcription Factors Reb1, Abf1, and Rap1**

(A) Experimental scheme. Yeast harboring MNase fused to the TFs Reb1, Abf1, or Rap1 were released from G1 arrest (left). The released cultures were sampled at 3-min time intervals and processed for mapping TF binding patterns. Synchronized progression was verified by DNA staining (right).

(B) TF binding profiles are consistent between time points and repeats. Shown are the Pearson correlations of the sum of signal on promoters, between all samples, time points, and repeats. Correlation with previous datasets, generated using unsynchronized cultures (Zentner et al., 2015), are indicated with a red * (Figures S2A–S2C).

(C) Representative binding profile to target genes. Averaged binding intensities to the indicated gene promoters are shown, with the location of sequence-predicted binding motif (orange box). Grey background depicts nucleosomes pattern in logarithmic growth, as measured by MNase-seq (see also Figures S2E–S2G).

(D) Reb1, Abf1, and Rap1 bind to distinct sets of promoters. The 100 promoters showing the strongest binding by each TF were selected. The binding patterns to the 500 bp upstream to the TSS of the 300 selected promoters are shown. Note the limited overlap between binding of the different factors. See Figure S2D for all targets of each TF.

(E) Binding of Reb1, Abf1, and Rap1 along gene promoters. Genes were aligned by their TSS. Shown is the average binding to all gene promoters (top) and the distribution of distances between the location of the maximal binding signal at each promoter to the TSS (bottom).

depletion of Pol II that is associated with the passing of the replication fork, suggesting that, if evicted, it regains binding rapidly.

Next, we asked if, following the passing of the replication fork, the increase in DNA content results in increased relative Pol II binding. To this end, we first quantified the progression of replication at each time point. We did this by examining the correlation between DNA content at each genomic region and the replication time (ToR) of this region. At early (G1) or late (G2/M) time points, the DNA content was uniform, independent of ToR. In contrast, at intermediate time points (e.g., 27 min) DNA content increased in proportion to ToR (Figures 1D and S1F). The extent to which the DNA content increases with ToR, therefore, defines the replication-dependent dosage bias (Figure 1E) and, accordingly, the expected increase in relative Pol II binding: if no buffering occurs and Pol II increases precisely in proportion to DNA content, its dependency on ToR will mimic that of the DNA content. If, on the other hand, its binding is buffered against the dosage changes, it will remain independent of ToR throughout the time course. Indeed, applying this approach to re-analyze data of mRNA synthesis rates in wild-type cells and in Δ*rtt109* mutants that lose transcription buffering (Voichek et al., 2016) captures the proportionality between transcription rates and DNA dosage in the Δ*rtt109* mutant and the minor dependency of mRNA synthesis rate on DNA dosage in wild-type cells (Figure 1F).

Quantifying the dependency of Pol II binding on DNA dosage (Figure 1E), we find that the relative Pol II binding to replicated DNA increased by only ~20% relative to the increase in DNA content, similar to the change in mRNA synthesis observed in wild-type cells (Figures 1E and 1F). Therefore, during unperturbed S phase, limited Pol II binding to replicated DNA fully accounts for the buffering of transcription rates. Note that this limited increase in Pol II binding differs from that found in cells arrested in mid-S-phase following hydroxyurea (HU) treatment (Voichek et al., 2018). In this latter case, the prolonged arrest, coupled with additional epigenetic changes, does allow a ~40% increase in Pol II binding to replicated DNA. Transcription buffering also remains highly efficient in this case but requires additional compensation processes triggered by the DNA replication checkpoint.

## Transient Depletion of TFs from Replicated DNA

Pol II is recruited to DNA by specific TFs that bind to *cis*-regulatory elements in promoter regions. We asked whether, similar to Pol II, TF binding to DNA is also insensitive to DNA dosage. To examine that, we chose three factors of general regulatory roles that bind a large number of targets at distinct genomic regions: Reb1, Abf1, and Rap1 (Yarragudi et al., 2004; Bai et al., 2011; Ganapathi et al., 2011).

To define the binding dynamics of these TFs during S phase, we released cells from G1 arrest and followed their progression along S phase, sampling the culture at 3-min time intervals. Synchronized progression was verified using DNA staining

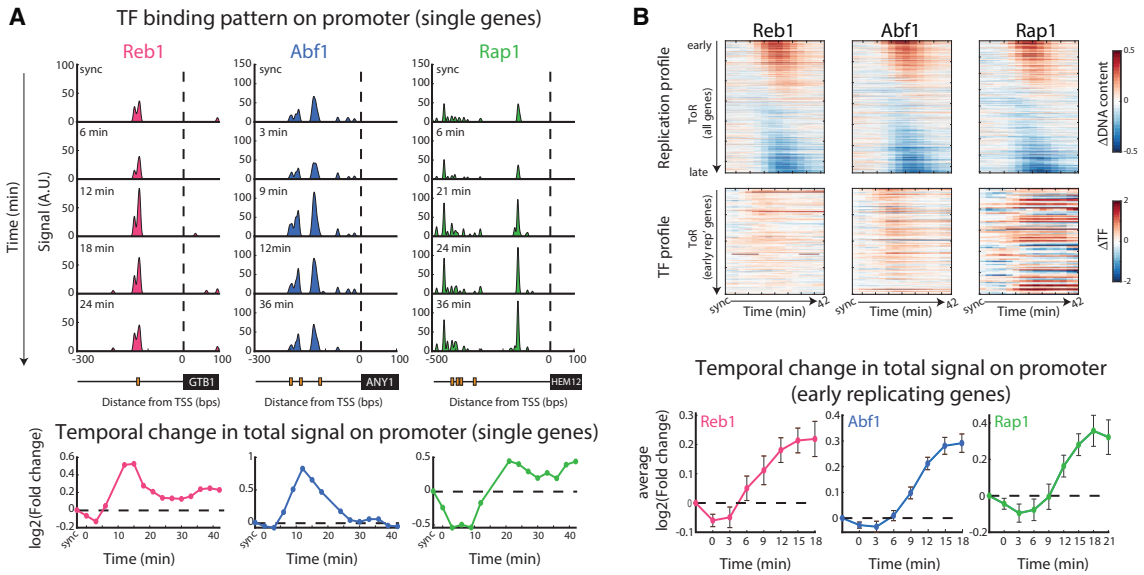


**Figure 3. Transient Eviction of TFs from Replicated DNA**

(A) Temporal changes in TF binding intensities at individual promoters. Representative examples of the binding dynamics and patterns on promoters. The binding upstream of the TSS is shown (top), with the predicted binding motifs marked (orange, middle). The signal over the of 500 bp upstream of the TSS was summed, and the temporal change was calculated by normalizing by the synchronized time point (bottom).

(B) Temporal dynamics of all bound promoters. Bound promoters (targets; see STAR Methods) were ordered according to their ToR. The top panel shows the replication profile of each gene, as calculated by measuring the ($log_2$) fold change in DNA signal on a 10-kB region around each gene and compared to the synchronized time point (top). The middle panel depicts the TF binding signal over the 500 bp upstream of the gene's TSS, of the 200 earliest-replicating target genes for Reb1 and Abf1, and the 100 earliest-replicating target genes for Rap1. The average TF signal along time and SE, over the same genes, are presented in the bottom panel.

(Figure 2A). TF binding was measured by chromatin endonuclease cleavage followed by sequencing (ChEC-Seq) (Schmid et al., 2004; Zentner et al., 2015). Binding profiles were highly correlated between repeats and time points and were consistent with previous data of the same factors in unsynchronized cultures (Figure 2B; Figure S2) (Zentner et al., 2015). Consistent with previous works, Reb1 and Abf1 were found preferentially ~130 bp upstream of the transcription start site (TSS), whereas Rap1 showed a more dispersed pattern along promoters (Figures 2C–2E and S2) (Bosio et al., 2017). Representative examples of TF binding dynamics is shown in Figure 3A. Focusing on early replicating regions, we noted a transient depletion of TFs during early replication (Figure 3B). This reduced abundance lasted for 3–6 min for all three TFs and was more pronounced than that observed for Pol II. Therefore, it appears that TFs are evicted from regions that are being replicated, presumably to prevent collisions with the DNA replication machinery, and then re-bind within minutes after this eviction.

### TF Binding to Replicated DNA Increases in Proportion to the Increase in DNA Dosage

Next, we examined whether, following their transient eviction, the binding of TFs to replicated promoters increases with the increasing DNA content. Using the ToR-based analysis described above (Figure 1D), we find that all three factors show biased binding to replicated DNA (Figures 4A and S3). Thus, binding of Rap1 and Reb1 to replicated DNA increased in proportion to the increase in DNA content, and the increase in DNA binding of Abf1 surpassed the increase in DNA dosage by ~50%. The post-replication chromatin environment is, therefore, permissive for TF binding and may, in fact, become more accessible for binding of certain factors, such as Abf1. When repeating the analysis for Pol II binding, focusing on the gene targets of each TF (Figure S3F), we find similar dynamics to those observed in our global analysis (Figure 1E), and thus, Pol II binding to replicated genes is inhibited.

The increased binding of TFs to replicated regions contrasts the suppression of Pol II binding and gene transcription from these regions. Still, we asked whether this binding increases even more in mutants that are deficient in transcription buffering. To test that, we examined the S-phase binding patterns of Abf1 and Reb1 in cells deleted of the histone acetyltransferase *RTT109*. Both factors showed the same binding dynamics observed in wild-type cells (Figures S3D and S3E). Thus, although H3K56ac suppresses transcription from replicated DNA, it does not affect TF binding.

## DISCUSSION

Differential binding of regulatory proteins to DNA is critical for the ability of a single genome to dictate different phenotypes. DNA replication challenges this organization in at least three ways. First, the passing of the replication machinery requires the removal of obstacles that may impede fork progression. Second, new histones, introduced for wrapping the newly synthesized DNA, carry a unique set of marks, which could influence regulatory factor binding. Finally, the changes in the relative abundance

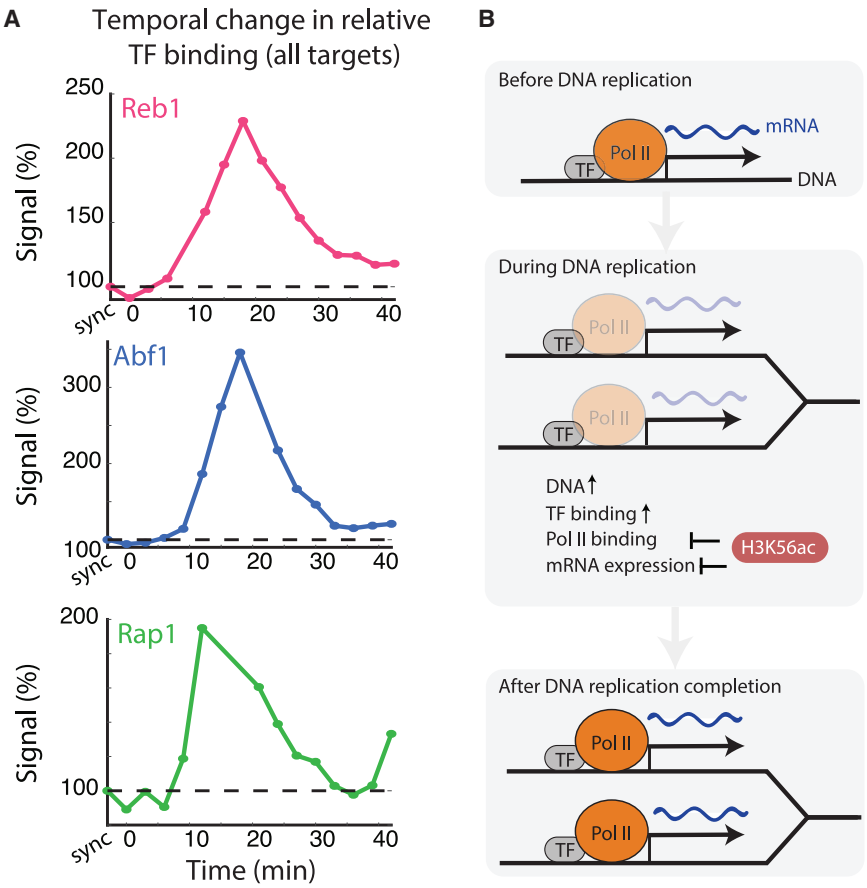


**Figure 4. TF Binding to Replicated DNA Increases with the Increasing DNA Content**

(A) Increasing TF binding intensity with increasing DNA dosage. Shown is the binding profile of each TF over its corresponding set of target genes. The binding was summed on the promoter region. The dependency of TF binding on ToR along time was calculated for each time point, as in Figure 1E. See also Figure S3 for TF binding in Δ*rtt109* cells. Analysis of Pol II binding over the same gene set is shown in Figure S3F.

(B) Model. Prior to DNA replication, TFs bind their target promoters and recruit Pol II and mRNA is transcribed. During replication, TFs are temporarily evicted from the DNA but then re-bind rapidly to the replicated DNA, poised to activate transcription. Despite TF binding to the replicated promoters, Pol II is not recruited to replicated genes, resulting in buffering of the imbalance in gene dosage that occurs during S phase.

of different genomic regions, introduced by differences in their replication timing, may draw regulatory proteins preferentially to early-replicating regions at the expense of late-replicating ones. We recently showed that these biases have little effect on gene expression, both during normal S phase and in cells arrested with their genome partially replicated (Voichek et al., 2016, 2018). Here, we examined how these biases affect proteins that bind DNA to regulate transcription: Pol II and specific TFs.

Previous studies indicated that during replication stress, such as HU treatment, Pol II is evicted from the DNA for ~60 min (Poli et al., 2016). Our genome-wide analysis of Pol II binding during normal S phase revealed a highly stable pattern, with little, if any, detectable depletion upon the passing of the replication fork. Our time resolution (3 min) cannot resolve whether Pol II is transiently evicted and rebinds rapidly or whether it remains in the close vicinity of the replication fork. In either case, the passing of the replication fork does not significantly perturb the overall Pol II binding pattern, neither in the promoters, where it awaits initiation signals, nor within the coding regions, where it is actively elongating transcripts. Previous studies also proposed that specific TFs are evicted from the DNA during replication, based on the pattern of protected DNA fragments (Ramachandran and Henikoff, 2016) or the transient inaccessibility of chromatin during DNA replication, as recently measured by ATAC-seq (Stewart-Morgan et al., 2019). In addition, by motif analysis, TFs were correlated with Okazaki fragment processing, implying that TFs may bind replicated DNA rapidly (Smith and Whitehouse, 2012). However, neither the identity of evicted factors nor the eviction dynamics were described. Our data, examining specific TFs with a wide spectrum of targets, did indicate such an eviction, showing a depletion of these factors from early-replicated regions that was more pronounced than that observed for Pol II. This depletion, however, is transient, lasting only several minutes.

Following the passing of the replication fork, DNA dosage increases, and it is present within a unique chromatin environment, characterized by a distinct pattern of histone marks. We asked whether replicated DNA remains accessible for binding regulatory factors. Previous studies suggested that the unique chromatin environment characterizing replicated DNA is less permissive for Pol II binding, as replicated promoters are transiently occupied by nucleosomes (Fennessy and Owen-Hughes, 2016; Ramachandran and Henikoff, 2016; Vasseur et al., 2016). Consistent with that, we find that Pol II remains largely insensitive to the increase in DNA content, showing only a limited increase in binding to replicated regions. However, the kinetics by which promoters regain the correct nucleosome positioning appears too rapid to explain the persistent suppression of Pol II binding. Furthermore, TF binding to replicated promoters does increase with the increasing DNA content. Therefore, the replication-dependent chromatin environment remains permissive for binding of TFs. Of note, for one of these factors, binding to replicated regions surpassed the increase in DNA content, suggesting that it binds replicated DNA with increased efficiency. This excessive binding may explain the transcriptional spike upon mitotic exit that was recently observed in human cells (Vaňková Hausnerová and Lanctôt, 2017).

Taken together, our work provides new insight into the dynamics of Pol II and of specific TFs during DNA replication. Although TFs are evicted from the DNA during replication, they regain binding rapidly and are poised on replicated promoters to initiate transcription in the daughter cells. The unique chromatin environment during replication, however, limits the ability of these factors to recruit Pol II to these replicated genes, explaining the observed buffering of the gene dosage imbalance at the level of mRNA expression (Figure 4B).

## STAR★METHODS

Detailed methods are provided in the online version of this paper and include the following:

- KEY RESOURCES TABLE
- LEAD CONTACT AND MATERIALS AVAILABILITY
- EXPERIMENTAL MODEL AND SUBJECT DETAILS
  - Budding yeast growth, maintenance, and genetic manipulation
- METHOD DETAILS
  - ChEC-Seq during the cell cycle
  - MNase-Seq
  - Flow cytometry
- QUANTIFICATION AND STATISTICAL ANALYSIS
  - Gene expression data and analysis
  - RNA Pol II ChIP-Seq and genomic DNA data
  - ChEC-Seq processing and analysis
  - Metagene profiles
  - Motif analysis
  - Quantifying signal along DNA replication
  - Time of replication (ToR) and gene groups
- DATA AND CODE AVAILABILITY

## SUPPLEMENTAL INFORMATION

Supplemental Information can be found online at https://doi.org/10.1016/j.celrep.2020.02.114.

## ACKNOWLEDGMENTS

We thank O. Lupo, Y. Gordon, Y. Voichek, and M. Carmi for technical assistance. We also thank members of our laboratory for fruitful discussions and comments on the project. This work was supported by the ISF and Minerva.

## AUTHOR CONTRIBUTIONS

R.B.-Z. and N.B. conceived the study and designed experiments; R.B.-Z, S.B., and M.C. performed experiments; R.B.-Z. and S.B. analyzed the data; R.B.-Z., S.B., and N.B. wrote the manuscript; N.B. supervised the research.

## DECLARATION OF INTERESTS

The authors declare no competing interests.

Received: October 7, 2019
Revised: January 13, 2020
Accepted: February 27, 2020
Published: March 24, 2020

## REFERENCES

Alabert, C., Barth, T.K., Reverón-Gómez, N., Sidoli, S., Schmidt, A., Jensen, O.N., Imhof, A., and Groth, A. (2015). Two distinct modes for propagation of histone PTMs across the cell cycle. Genes Dev. *29*, 585–590.

Bai, L., Ondracka, A., and Cross, F.R. (2011). Multiple sequence-specific factors generate the nucleosome-depleted region on CLN2 promoter. Mol. Cell *42*, 465–476.

Bannister, A.J., and Kouzarides, T. (2011). Regulation of chromatin by histone modifications. Cell Res. *21*, 381–395.

Bar-Ziv, R., Voichek, Y., and Barkai, N. (2016a). Chromatin dynamics during DNA replication. Genome Res. *26*, 1245–1256.

Bar-Ziv, R., Voichek, Y., and Barkai, N. (2016b). Dealing with Gene-Dosage Imbalance during S Phase. Trends Genet. *32*, 717–723.

Blecher-Gonen, R., Barnett-Itzhaki, Z., Jaitin, D., Amann-Zalcenstein, D., Lara-Astiaso, D., and Amit, I. (2013). High-throughput chromatin immunoprecipitation for genome-wide mapping of *in vivo* protein-DNA interactions and epigenomic states. Nat. Protoc. *8*, 539–554.

Bosio, M.C., Fermi, B., Spagnoli, G., Levati, E., Rubbi, L., Ferrari, R., Pellegrini, M., and Dieci, G. (2017). Abf1 and other general regulatory factors control ribosome biogenesis gene expression in budding yeast. Nucleic Acids Res. *45*, 4493–4506.

Chen, X., Hughes, T.R., and Morris, Q. (2007). RankMotif++: a motif-search algorithm that accounts for relative ranks of K-mers in binding transcription factors. Bioinformatics *23*, i72–i79.

David, L., Huber, W., Granovskaia, M., Toedling, J., Palm, C.J., Bofkin, L., Jones, T., Davis, R.W., and Steinmetz, L.M. (2006). A high-resolution map of transcription in the yeast genome. Proc. Natl. Acad. Sci. USA *103*, 5320–5325.

Driscoll, R., Hudson, A., and Jackson, S.P. (2007). Yeast Rtt109 promotes genome stability by acetylating histone H3 on lysine 56. Science *315*, 649–652.

Fennessy, R.T., and Owen-Hughes, T. (2016). Establishment of a promoter-based chromatin architecture on recently replicated DNA can accommodate variable inter-nucleosome spacing. Nucleic Acids Res. *44*, 7189–7203.

Ganapathi, M., Palumbo, M.J., Ansari, S.A., He, Q., Tsui, K., Nislow, C., and Morse, R.H. (2011). Extensive role of the general regulatory factors, Abf1 and Rap1, in determining genome-wide chromatin structure in budding yeast. Nucleic Acids Res. *39*, 2032–2044.

Garber, M., Yosef, N., Goren, A., Raychowdhury, R., Thielke, A., Guttman, M., Robinson, J., Minie, B., Chevrier, N., Itzhaki, Z., et al. (2012). A high-throughput chromatin immunoprecipitation approach reveals principles of dynamic gene regulation in mammals. Mol. Cell *47*, 810–822.

Gasch, A.P., Spellman, P.T., Kao, C.M., Carmel-Harel, O., Eisen, M.B., Storz, G., Botstein, D., and Brown, P.O. (2000). Genomic expression programs in the response of yeast cells to environmental changes. Mol. Biol. Cell *11*, 4241–4257.

Gietz, R.D., Schiestl, R.H., Willems, A.R., and Woods, R.A. (1995). Studies on the transformation of intact yeast cells by the LiAc/SS-DNA/PEG procedure. Yeast *11*, 355–360.

Grant, C.E., Bailey, T.L., and Noble, W.S. (2011). FIMO: scanning for occurrences of a given motif. Bioinformatics *27*, 1017–1018.

Han, J., Zhou, H., Horazdovsky, B., Zhang, K., Xu, R.M., and Zhang, Z. (2007). Rtt109 acetylates histone H3 lysine 56 and functions in DNA replication. Science *315*, 653–655.

Ihmels, J., Friedlander, G., Bergmann, S., Sarig, O., Ziv, Y., and Barkai, N. (2002). Revealing modular organization in the yeast transcriptional network. Nat. Genet. *31*, 370–377.

Ihmels, J., Bergmann, S., and Barkai, N. (2004). Defining transcription modules using large-scale gene expression data. Bioinformatics *20*, 1993–2003.

Janke, C., Magiera, M.M., Rathfelder, N., Taxis, C., Reber, S., Maekawa, H., Moreno-Borchart, A., Doenges, G., Schwob, E., Schiebel, E., and Knop, M. (2004). A versatile toolbox for PCR-based tagging of yeast genes: new fluorescent proteins, more markers and promoter substitution cassettes. Yeast *21*, 947–962.

Liu, C.L., Kaplan, T., Kim, M., Buratowski, S., Schreiber, S.L., Friedman, N., and Rando, O.J. (2005). Single-nucleosome mapping of histone modifications in *S. cerevisiae*. PLoS Biol. *3*, e328.

MacAlpine, D.M., and Almouzni, G. (2013). Chromatin and DNA replication. Cold Spring Harb. Perspect. Biol. *5*, a010207.

Padovan-Merhar, O., Nair, G.P., Biaesch, A.G., Mayer, A., Scarfone, S., Foley, S.W., Wu, A.R., Churchman, L.S., Singh, A., and Raj, A. (2015). Single mammalian cells compensate for differences in cellular volume and DNA copy number through independent global transcriptional mechanisms. Mol. Cell *58*, 339–352.

Poli, J., Gerhold, C.B., Tosi, A., Hustedt, N., Seeber, A., Sack, R., Herzog, F., Pasero, P., Shimada, K., Hopfner, K.P., and Gasser, S.M. (2016). Mec1, INO80, and the PAF1 complex cooperate to limit transcription replication conflicts through RNAPII removal during replication stress. Genes Dev. *30*, 337–354.

Ramachandran, S., and Henikoff, S. (2016). Transcriptional Regulators Compete with Nucleosomes Post-replication. Cell *165*, 580–592.

Ramachandran, S., Ahmad, K., and Henikoff, S. (2017). Capitalizing on disaster: Establishing chromatin specificity behind the replication fork. BioEssays *39*, 1600150.

Schmid, M., Durussel, T., and Laemmli, U.K. (2004). ChIC and ChEC; genomic mapping of chromatin proteins. Mol. Cell *16*, 147–157.

Slager, J., and Veening, J.-W. (2016). Hard-Wired Control of Bacterial Processes by Chromosomal Gene Location. Trends Microbiol. *24*, 788–800.

Smith, D.J., and Whitehouse, I. (2012). Intrinsic coupling of lagging-strand synthesis to chromatin assembly. Nature *483*, 434–438.

Stewart-Morgan, K.R., Reverón-Gómez, N., and Groth, A. (2019). Transcription Restart Establishes Chromatin Accessibility after DNA Replication. Mol. Cell *75*, 284–297.e6.

Vaňková Hausnerová, V., and Lanctôt, C. (2017). Transcriptional Output Transiently Spikes Upon Mitotic Exit. Sci. Rep. *7*, 12607.

Vasseur, P., Tonazzini, S., Ziane, R., Camasses, A., Rando, O.J., and Radman-Livaja, M. (2016). Dynamics of Nucleosome Positioning Maturation following Genomic Replication. Cell Rep. *16*, 2651–2665.

Voichek, Y., Bar-Ziv, R., and Barkai, N. (2016). Expression homeostasis during DNA replication. Science *351*, 1087–1090.

Voichek, Y., Mittelman, K., Gordon, Y., Bar-Ziv, R., Lifshitz Smit, D., Shenhav, R., and Barkai, N. (2018). Epigenetic Control of Expression Homeostasis during Replication Is Stabilized by the Replication Checkpoint. Mol. Cell *70*, 1121–1133.e9.

Yabuki, N., Terashima, H., and Kitada, K. (2002). Mapping of early firing origins on a replication profile of budding yeast. Genes Cell *7*, 781–789.

Yarragudi, A., Miyake, T., Li, R., and Morse, R.H. (2004). Comparison of ABF1 and RAP1 in chromatin opening and transactivator potentiation in the budding yeast *Saccharomyces cerevisiae*. Mol. Cell. Biol. *24*, 9152–9164.

Yunger, S., Rosenfeld, L., Garini, Y., and Shav-Tal, Y. (2010). Single-allele analysis of transcription kinetics in living mammalian cells. Nat. Methods *7*, 631–633.

Zentner, G.E., Kasinathan, S., Xin, B., Rohs, R., and Henikoff, S. (2015). ChEC-seq kinetics discriminates transcription factor binding sites by DNA sequence and shape *in vivo*. Nat. Commun. *6*, 8733.

## STAR★METHODS

### KEY RESOURCES TABLE

| REAGENT or RESOURCE | SOURCE | IDENTIFIER |
|---|---|---|
| Chemicals, Peptides, and Recombinant Proteins | | |
| Yeast Mating Factor Alpha, Acetate Salt | US Biological Life Sciences | Cat#59401-28-4 |
| cOmplete, EDTA-free Protease Inhibitor Cocktail | Sigma Aldrich | Cat#11873580001 |
| Proteinase K | Sigma Aldrich | Cat#P2308 |
| RNase A | Sigma Aldrich | Cat#4875 |
| AMPure XP | Beckman Coulter | Cat#A63881 |
| Micrococcal nuclease (MNase) | Worthington | Cat#LS004797 |
| SYBR® Green I nucleic acid gel stain | Sigma Aldrich | Cat#S9430 |
| Critical Commercial Assays | | |
| Total RNA Isolation Nucleospin 96 | Macherey-Nagel | Cat#740709 |
| HiYield Plasmid Mini Kit | RBC Bioscience | Cat#YPD100 |
| Deposited Data | | |
| ChEC-Seq and Mnase-Seq data | This study | SRA database, BioProject PRJNA542378 |
| Yeast reference genome version R64-1-1 | SGD | https://downloads.yeastgenome.org/sequence/S288C_reference/genome_releases/S288C_reference_genome_R64-1-1_20110203.tgz |
| Experimental Models: Organisms/Strains | | |
| *REB1-MNase* (BY4741 MATa, his3-1, leu2-0, met15-0, N/A ura3-0, REB1-3FLAG-MNase-kanMX6) | This study | N/A |
| *ABF1-MNase* (BY4741 MATa, his3-1, leu2-0, met15-0, N/A ura3-0, ABF1-3FLAG-MNase-kanMX6) | This study | N/A |
| *RAP1-MNase* (BY4741 MATa, his3-1, leu2-0, met15-0, N/A ura3-0, RAP1-3FLAG-MNase-kanMX6) | This study | N/A |
| *REB1-MNase rtt109Δ* (BY4741 MATa, his3-1, leu2-0, met15-0, N/A ura3-0, REB1-3FLAG-MNase-kanMX6, rtt109::Hyg) | This study | N/A |
| *ABF1-MNase rtt109Δ* (BY4741 MATa, his3-1, leu2-0, met15-0, N/A ura3-0, ABF1-3FLAG-MNase-kanMX6, rtt109::Hyg) | This study | N/A |
| WT (BY4741 MATa, his3-1, leu2-0, met15-0, N/A ura3-0) | S288C-derived strain, parental strain for the Euroscarf MATa haploid gene deletion collection | BY4741 |
| Oligonucleotides | | |
| Primers used for strain creation | This study | Table S2 |
| Recombinant DNA | | |
| pGZ108 (pFA6a-3FLAG-MNase-kanM6) | Addgene | Cat #70231 |
| pYM24 | Euroscarf | Cat #P30236 |
| Software and algorithms | | |
| bowtie | Johns Hopkins University | http://bowtie-bio.sourceforge.net/ |

## LEAD CONTACT AND MATERIALS AVAILABILITY

All strains used in this study are available by direct request to the lead contact. Further information and requests for resources and reagents should be directed to and will be fulfilled by the lead contact, Dr. Naama Barkai (naama.barkai@weizmann.ac.il).

## EXPERIMENTAL MODEL AND SUBJECT DETAILS

All strains used are derived from the wild-type *Saccharomyces cerevisiae* strain, BY4741, and specific genotypes of all strains used in this study are available in the Key Resources Table. Growth conditions are specified under each experimental method detailed below.

### Budding yeast growth, maintenance, and genetic manipulation

Yeast strains were freshly thawed before experiments from a frozen stock, plated on YPD plates, and grown. Single colonies were picked and grown at 30°C in liquid YPD medium. Optical density measurements of the different experiments are specified in the Method Details section.

For genetic manipulation of yeast, BY4741 strain, of genotype *MATa his3-Δ1 leu2-Δ0 lys2-Δ0 met15-Δ0 ura3-Δ0* was transformed using the LiAc/SS DNA/PEG method (Gietz et al., 1995). Briefly, a single colony was inoculated into fresh YPD and was grown to $OD_{600}$ of 0.5. Cells were then washed three times with DDW and once with LiAc 100mM. Cells were then resuspended in transformation mix (33% PEG3350, 100mM LiAc, single stranded salmon sperm DNA and the DNA fragment intended for transformation). The cells were incubated at 30°C for 30 minutes followed by a 30 minutes heat shock (42°C). Cells were then grown in YPD liquid culture for overnight recovery and then plated on the appropriate selection plate.

For tagging specific transcription factors, MNase was amplified from a cassette from pGZ108 (Zentner et al., 2015), and selected on plates with G418. Reb1-MNase and Abf1-MNase strains were further transformed with a PCR fragment amplified from pYM24 (Janke et al., 2004) to delete *RTT109* (Figure S3) replacing the gene's ORF by transformation. These strains were grown on plates containing G418 and Hygromycin B. For the MNase-seq experiments the wild-type *Saccharomyces cerevisiae*, BY4741, was used. The generated strains were verified first using PCR and gel electrophoresis, and then further verified using DNA sequencing.

## METHOD DETAILS

### ChEC-Seq during the cell cycle

Cell cycle synchronization using α-factor was done as previously described (Bar-Ziv et al., 2016a). Briefly, cells were grown in liquid YPD overnight at 30°C and diluted in fresh medium, to allow several divisions in fresh YPD. When reaching an $OD_{600}$ of 0.12, cells were washed from the media by centrifugation (3000 rpm, 5 min). Cells were then resuspended in an equal volume of fresh warm YPD with α-factor to a final concentration of 5 μg/mL. Next, each yeast culture was divided into 16 (experiment set #1; Figures 4A, S3D, and S3E) or 4 (experiment set #2; Figures S3B and S3C) separate 50-mL tubes with a ventilated cap (CELLSTAR CELL reactor filter top tube, Greiner Bio-One, 227245), each containing 35 mL of yeast culture. Each tube contained the material used for ChEC-Seq in a single time-point and DNA staining for flow cytometry. Cells were incubated for 3 hours at 30°C with α-factor in an incubator and then transferred to a water bath orbital shaker 30 min before the end of synchronization (MRC, WBT-450). Every 3 min for 42 min, one tube was taken out of the bath orbital shaker and washed twice from α-factor by centrifugation (4000 rpm, 1 min) and resuspension in fresh, warm YPD. Following two washes, cells were resuspended in an equal volume of fresh, warm YPD and returned to the bath shaker to grow at 30°C. The first sample returned to the bath shaker is the last sample in the time-course (first released–last time-point in time-course). The second-to-last sample in the time-course was released and immediately processed, termed the "0 minutes" sample. The last sample in the time-course was not released from α-factor and was termed "synchronized." Following release from synchronization, 0.5 mL of each sample was aliquoted to a different tube to be used for DNA staining and flow cytometry. Samples for DNA staining were centrifuged for 10 s in 13,000 rpm, sup was discarded, and pellet was resuspended and fixated with 70% ethanol. The remaining culture was used for ChEC-Seq, as described previously (Zentner et al., 2015), with minor modifications. Briefly, cells were pelleted at 1500 g, transferred to a deep-well 96-well plate, and then washed three times with 1 ml Buffer A (15 mM Tris pH 7.5, 80 mM KCl, 0.1 mM EGTA, 0.2 mM spermine, 0.5 mM spermidine, 1 × Roche cOmplete EDTA-free mini protease inhibitors, 1 mM PMSF). Cells were then resuspended in 200 μL Buffer A containing 0.1% digitonin and permeabilized at 30 °C for 5 min. $CaCl_2$ was added to a final concentration of 2 mM for 30 s at 30°C. Next, stop buffer (400 mM NaCl, 20 mM EDTA, 4 mM EGTA) and 1% SDS was added and vortexed. Proteinase K (100 μg, Sigma-Aldrich) was then added and incubated at 55°C for 30 min. Subsequent nucleic acids isolation, RNase A treatment, and DNA clean-ups were done as previously described (Zentner et al., 2015). For the second set of experiments (Figure S3), small adjustments were made in the library preparation in order to increase yield: Reverse SPRI clean-up for enrichment of small DNA fragments was done (0.8X). Ethanol precipitation was performed during the clean-up steps instead of using S300 spin columns (120uL EtOH 96% and 5uL of Sodium acetate (3M) were added to ~50 uL of sample, vortexed and precipitated at −80C for > hour), followed by a final SPRI cleanup (1X). ChEC libraries were indexed (Garber et al., 2012), pooled and sequenced on Illumina NextSeq500 for single 50bps reads.

### MNase-Seq

For profiles of nucleosome occupancy in logarithmic growth, MNase-seq was performed as previously described (Liu et al., 2005). Cells were grown over night, then diluted and grown for 5-6 hours shaking at 30°C to reach $OD_{600}$ of 0.5. 10ml of cells were fixated for 15 min in 1% formaldehyde shaking in RT. Cell pellets were washed, and treated with zymolyase (Amsbio, 120493-1) for 25 minutes in 30°C to generate spheroplasts. Then, spheroplasts were subjected to MNase digestion (Worthington, LS004797) for 20 minutes in 37°C. MNase treatment was stopped using a stop buffer (220mM NaCl, 0.2% SDS, 0.2% sodium deoxycholate, 10mM EDTA, 2% Triton X-100). Cells were reverse cross linked: RNase (Sigma, R4875) treatment in 37°C for 30 min and then Proteinase K (Sigma P2308) in 37°C for 2 hours. Samples were incubated overnight at 65°C and DNA was purified using SPRI beads with a ratio of 2X. DNA libraries were indexed (Blecher-Gonen et al., 2013) pooled and pair-end sequenced on Illumina NextSeq500.

### Flow cytometry

To verify cell-cycle synchronization efficiency and position along the cell cycle, we performed DNA staining of samples from each time-point using flow cytometry. Briefly, cells were washed twice with 50 mM Tris-HCl (pH = 8), resuspended in RNase A for 40 min in 37°C, washed twice with 50 mM Tris-HCl (pH = 8), and resuspended in Proteinase K for 1 h incubation at 37°C. Then, cells were washed twice again, resuspended in SYBR green (S9430, Sigma-Aldrich; 1:1000), and incubated in the dark at room temperature for 1 h. Then, cells were washed from the stain and resuspended in 50 mM Tris-HCl (pH 8) and sonicated in the Diagenode Bioruptor for three cycles of 10 s on and 20 s off in low intensity. Finally, cells were taken to FACS for analysis using the BD LSRII system (BD Biosciences). We note that time points 0 & 12 for Abf1-MNase time course are missing, as these FACS staining measurements failed.

## QUANTIFICATION AND STATISTICAL ANALYSIS

### Gene expression data and analysis

Gene expression data and mRNA synthesis rates for wild-type yeast (BY4741) and Δ*rtt109* measured along the cell-cycle following release from α-factor synchronization previously published by our lab was used (Voichek et al., 2016). Note, the experimental scheme and time points are the same as in the current study. Briefly, cells were released, after washing, from 3 hours in YPD with 5μg/mL α-factor into fresh YPD and samples for RNA-Seq and flow-cytometry were harvested, every 3 min for 39 min, and then every 6 minutes for a total of 135 min. Sequencing reads were mapped to the *S. cerevisiae* genome (SGD, R64-1-1) using Bowtie (parameters: –best –a –m 2 –strata –5 10). Reads mapped to rRNA were discarded. Expression of each gene was quantified as the sum of all reads aligned to the region between 400bp upstream of the 3′ end, and 200bp downstream of the 3′ end. Genes with high sequence similarity in this region were quantified according to the amount of uniquely mapped sequences (Voichek et al., 2016). Total expression was normalized to have a sum of $10^6$. Expression levels at each time-point were divided by the expression in the synchronized time-point, $\log_2$-transformed, and then averaged on the group of genes or single genes. Note that in Figure 1, experiments were executed separately; As each time course involves release from cell cycle synchronization, the time points between (E) and (F) are not directly comparable, due to slight temporal shifts.

### RNA Pol II ChIP-Seq and genomic DNA data

RNA Polymerase II and genomic DNA data along S-phase from a previously published dataset generated in our lab was used (Bar-Ziv et al., 2016a). Briefly, a wild-type yeast culture (W303) progressing synchronously following α-factor synchronization, was used. Cells were grown in 24°C, arrested by α-factor for 2.5 hours, and shifted to 34°C for half an hour before release from G1 arrest. At each time-point, 35 mL of yeast were used for ChIP-seq, with chromatin from 10 mL of culture used per antibody. Tubes were taken out of the bath shaker and fixated at the same time, as each sample has been released at a different time, in 3-min intervals. The antibody used to probe RNA Polymerase II is Pol II (CTD) 8WG16 (Covance, MMS-126R). The cells were fixated and processed further as previously described. Samples were harvested from the synchronized culture, and then from 6 min after release taken every 3 min for 45 min total after release from synchronization. Reads were aligned using Bowtie (parameters: –best –m 1) to a combined *S. cerevisiae* and *S. pombe* genome. This experimental scheme, that used spiked-in *S. pombe,* was not used in other experiments presented here. The spike-in method was an experimental method that was used to probe total levels of chromatin marks in our previous study, but was not needed for calculations in the current study (see note in Bar-Ziv et al., 2016a). Genomic tracks were calculated by extending the aligned reads to cover 200 bp and adding +1 to each covered location. All tracks were normalized to have a total signal of 1,000,000. We note that as we are using sequencing methods, we measure the relative levels of DNA/Pol II. As replication profiles are measured using sequencing, late replicating genes show a relative decrease in signal when early genes are replicated. Each separate experiment can quantify relative differences between different loci in the genome, but total levels are assumed to stay the same. Thus, a real increase in one location might create a seemingly decrease of non-changing positions. For analysis of Pol II binding by ToR bias, regulated genes were taken out of the analysis (as in Voichek et al., 2016). This group of genes includes cell cycle genes (“cell-cycle (G1),” “cell cycle(G2/M)” and “cell cycle(CDC15)“), genes regulated in response to mating-factor synchronization (“mating”) and genes responding to stressed condition (“protein synthesis,” “stress,” ”rRNA processing,” “ESR induce” and “ESR reduce”) (Gasch et al., 2000; Ihmels et al., 2002). All genes are listed in Table S1.

### ChEC-Seq processing and analysis

Sequenced reads from ChEC-Seq experiments of each TF, along the time course in S-phase, were aligned using Bowtie2 to a *S. cerevisiae* genome (reference genome, cerR64). ChEC-Seq tracks representing the enrichment of every locus in the yeast genome were calculated for all samples. Genomic tracks were calculated by adding +1 to each genomic location corresponding to the first nucleotide in each read and normalized to have a total signal of 10,000,000 to control for sequencing depth. The signal on each promoter (500bps upstream of the TSS; David et al., 2006) was summed. Genes with a positive cumulative signal in their promoter above noise were defined as targets. For temporal dynamics, for each time point the total amount of signal was normalized, and the $\log_2$ fold change between each time point and the synchronized time point was calculated. Genes that were identified as targets were reproducible in previously published datasets (Figure S2). Several samples for experiment set #1 were discarded from further analysis due to technical issues, such as low alignment rate: Reb1-Mnase 9 min, Abf1 21-Mnase min, Rap1-Mnase 15&18 min, Reb1-Mnase *Δrtt109* 15&18&30 min, Abf1-Mnase *Δrtt109* 9&12&18 min. For analysis of TF binding by ToR bias, regulated genes were taken out of the analysis (as in Voichek et al., 2016).

### Metagene profiles

For Pol II binding, metagene analysis was done as follows: Taking the signal 500 bps upstream of the TSS for every gene in this profile (David et al., 2006). The signal found between the TSS and the transcription termination site (TTS) was binned into 50 equal-sized bins to be able to compare genes of different lengths. Signal for all genes was then separated according to expression levels, and averaged to get the average pattern. For TF binding, metagene analysis was done as follows: taking the signal 800 bp upstream of the transcription start site (TSS) for every gene in this profile, and 100 bps downstream of the TSS. Signal for all genes was averaged to get the average pattern.

### Motif analysis

For finding the motifs of TFs on the presented promoters, the top-scoring motif from The Yeast Transcription Factor Specificity Compendium (Chen et al., 2007) was searched along the gene's promoter using FIMO (Grant et al., 2011).

### Quantifying signal along DNA replication

To quantify the change in signal along DNA replication (as shown in Figures 1D–1G; Figure S1E), the $\log_2$ fold change of each gene (for Pol II, DNA replication, gene expression, and mRNA synthesis), compared to the synchronized time point, was plotted. The data was then fitted using first-degree polynomial fitting. The slope was then linearly transformed, so that the maximum increase in genomic DNA during replication would be 2. For Pol II, the signal on the promoter region (500 bps upstream of TSS), or the signal on the ORF was summed. For DNA content, the region of 10kB around the TSS of the gene was summed. For TFs, the same calculation was done, calculated only for target genes. For TFs, the binding was summed on the promoter, 500 bps upstream of the TSS. Note that "regulated genes" (see above, Table S1) were discarded from the quantification.

### Time of replication (ToR) and gene groups

Replication timing data of DNA from Yabuki et al. (2002) was used to define gene replication time by assigning each gene the replication time closest to its 5′ end. Gene groups for RNA analysis (Figure 1) G2/M genes and G1 genes were taken from Ihmels et al. (2004). For the histone gene group, all 8 histone genes were used.

## DATA AND CODE AVAILABILITY

The ChEC-seq and MNase-Seq datasets supporting the conclusions of this article are available in the NCBI Sequence Read Archives repository, accession number BioProject PRJNA542378.

**Cell Reports, Volume *30***

## Supplemental Information

# Transcription Factor Binding to Replicated DNA

**Raz Bar-Ziv, Sagie Brodsky, Michal Chapal, and Naama Barkai**

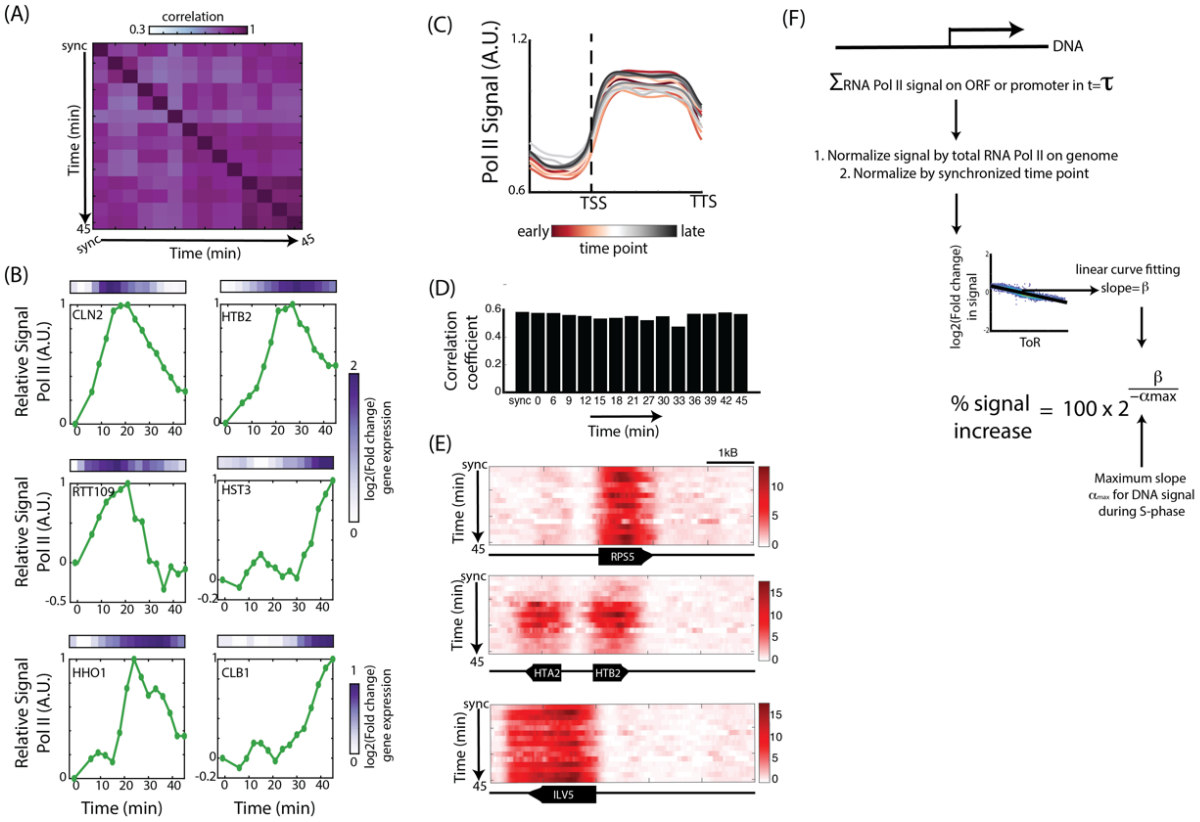


Figure S1: *The recruitment of RNA polymerase II (Pol II) to replicated DNA, Related to Figure 1.*

(A) *Correlations between data points:* The Pearson correlation between time points of samples of Pol II ChIP-Seq.

(B) *RNA Pol II binding to regulated genes:* Examples of the change in Pol II binding to regulated genes along the time course shows the expected cell-cycle dynamics; G1/late-G1 genes (*CLN2* and *RTT109*), S-phase histone genes (*HHO1* and *HTB1)*, and G2/M genes (*HST3* and *CLB1)*. The average ($\log_2$) fold change in binding dynamics of RNA Pol II to the indicated gene (ORF) was normalized by the synchronized time point and the maximum value along the time course (bottom), and the $\log_2$ fold change in mRNA levels of the gene (heatmap, top), upon release from α-factor synchronization, along the time course, normalized to the synchronized time point.

(C) *RNA Pol II binding across the cell-cycle:* Meta-gene analysis of each time point along the time course (for all genes). Genes were aligned by their transcription start and termination sites (TSS and TTS, respectively), and binned to control for variation in gene length (see Methods). Shown is the average profile.

(D) *Correlation of RNA Pol II binding with gene expression:* The Pearson correlation coefficient between the median gene expression levels in wild type cells across the cell cycle (as measured in RNA-seq) to the Pol II binding signal on the open reading frame (ORF) (as measured in ChIP-Seq).

(E) *RNA Pol II binding to specific loci:* Shown are the binding profiles of Pol II to a 5kB region of the genes *RPS5* (Chr X), *HTA2* AND *HTB2* (Chr II), and *ILV5* (Chr XII). Each row represents a different time point. Note that H2A2/HTB2 are histone genes that are induced during S-phase, and thus binding of Pol II increases in their region during the S-phase time points.

(F) *Calculating the dependency of RNA Pol II on time of replication:* For each time point τ, the Pol II signal on each ORF or promoter was summed, and normalized by the total signal of Pol II on the genome. Then, the signal was normalized to the synchronized time point, to get the fold-change increase in signal per gene. Next, the fold change in Pol II signal on all examined genes was plotted against their time of replication (ToR), and by linear curve fitting, the slope (per time point τ along the time course) was extracted. Finally, the slope of the curve was divided by the negative of the maximum slope (generated similarly for DNA content), and converted to percentages so that the synchronized time point is a 100%.

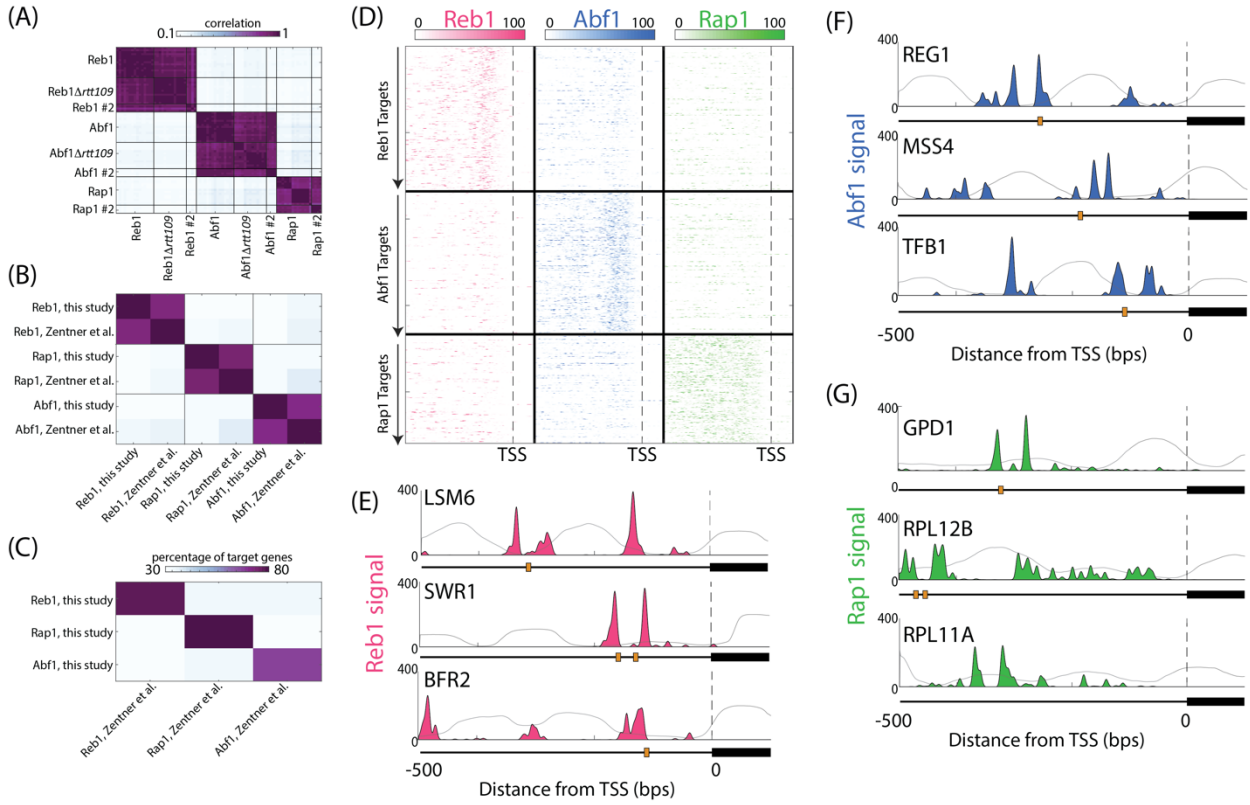


Figure S2: *Measuring the binding of transcription factors during DNA replication, Related to Figure 2.*

(A) *Correlations between experiments:* The signal on each promoter for each TF, in each time point, was summed and cross-correlated to all other samples.

(B) *Correlations with previous data* (Zentner et al., 2015)*:* Median sum on promoter of each TF was calculated, and then correlated to the binding data produced by Zentner et al. for yeast probed during logarithmic growth.

(C) The percentage of overlap in identified target genes (see Methods) for each TF in this study vs. Zentner et al, and between the different TFs, is shown.

(D) *Spatial binding patterns of TFs:* As Figure 2D, the spatial binding pattern to the 500 bps upstream to the TSS of the indicated TFs is shown, for all identified targets of each TF.

(E) *Single-gene examples:* As Figure 2C, the binding patterns of three target genes of each transcription factor are shown. The location of motifs in the promoter (orange box) and the transcript (black box) are indicated. Grey background signal represents the pattern of nucleosomes in logarithmic growth.

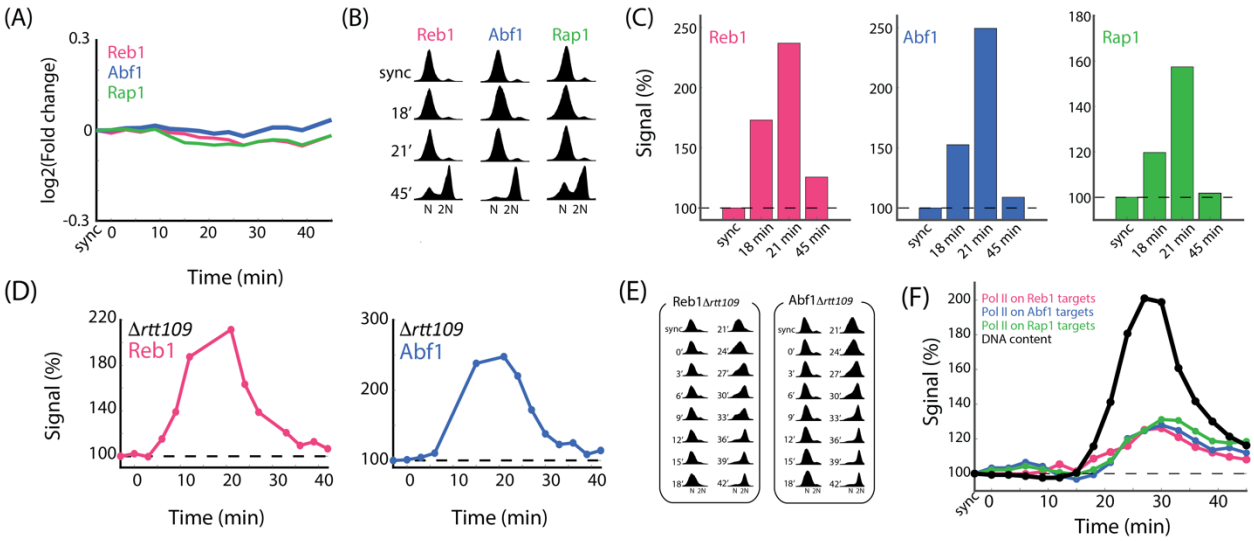


Figure S3: *TFs re-bind to replicated DNA, Related to Figure 4.*

(A) *Little fluctuations in gene expression of TF targets during S-phase*: The $\log_2$ fold change in expression levels in a wild type strain, as measured by RNA-seq, of the gene targets of each TF is shown. Data from Voichek et al., 2016.

(B) *Cell cycle progression:* Synchronized progression for results shown in Figure S4C. Cell cycle progression was verified by total DNA content profile using fluorescence-activated cell sorting (FACS).

(C) *TF binding to replicated DNA is not buffered:* The binding dynamics of each TF on all its targets was calculated as in Figure 1E (biological repeat #2).

(D) *Increasing TF binding intensity with increasing DNA dosage also in Δrtt109:* Same as Figure 1E for the indicated binding profiles. Synchronized progression was verified using DNA staining (E).

(F) *Minor sensitivity of RNA Pol II to gene dosage when examined only on gene targets of each transcription factor:* As in Figure 1E, shown are the dependencies of Pol II binding to ORFs on ToR along time. The analysis was done for the set of target-genes of each transcription factor.